Kinetic Model for the Chiral Symmetry Breaking Transition in the Growth Front of a Conglomerate Crystal Phase

Kouichi Asakura,*,† Yasushi Nagasaka,† Shuichi Osanai,† and Dilip K. Kondepudi‡

Department of Applied Chemistry, Faculty of Science and Technology, Keio University, 3-14-1, Hiyoshi, Kohoku, Yokohama 223-8522, Japan, and Department of Chemistry, Wake Forest University, Winston-Salem, North Carolina 27109

Received: July 7, 2004; In Final Form: October 29, 2004

In its molten phase, 1,1′-binaphthyl is racemic due to its high racemization rate, but it can crystallize as a conglomerate of *R* and *S* crystals. Our experiments have indicated that, under some conditions, the crystal growth front of 1,1′-binaphthyl shows many of the characteristics of an open system in which chiral symmetry is broken; i.e., the growing solid phase becomes predominantly *R* or *S*. Here we present a kinetic model to explain the observed chiral symmetry breaking. The model is based on growth due to attachment of *R* or *S* growth units to a crystal surface in a supercooled melt. Chiral symmetry breaking occurs due to chirally autocatalytic formation of *R* or *S* growth units on the growth surface. Unlike the many models suggested and studied in the 1980s, there is no cross-inhibition between *R*- and *S*-enantiomer in the model presented here. In our model, asymmetric and symmetric steady-state solutions that do not intersect were found. Through linear stability analysis, the critical point, at which a symmetric solution becomes unstable and makes a transition to an asymmetric solution, is determined.

Introduction

In the absence of a chiral influence, chemical reactions that generate chiral molecules from achiral reactants produce the two enantiomers at identical rates. That this does not imply that chemical processes will always generate equal amounts of enantiomers can be seen in nonequilibrium systems that exhibit spontaneous chiral symmetry breaking. Such a process might have caused the dominance of L-amino acids and D-sugars, a fundamental asymmetry in the chemistry of life. This nonequilibrium asymmetric state is maintained in open living systems through the flow of matter and energy. Though the exact mechanism that established this particular asymmetry is not known, it is now well-known that irreversible dissipative processes can give rise to states of broken symmetry in systems far from thermodynamic equilibrium.[1] Such states include states with large chiral asymmetry[2] as well as oscillations, propagating chemical waves, and spatial patterns.[3] These states have entropies that are lower than that of the corresponding equilibrium states and, in that sense, they are ordered.

Differential equations resulting from the kinetic model usually give us insight into the mechanism, generation, and maintenance of the ordered states. The Brusselator[4] and the FKN model[5] for oscillation[6] and Turing model[7] for spatial pattern formation[8] are the typical examples. For chiral symmetry breaking, Kondepudi and Nelson formulated a model in the 1980s[9,10] by extending a model originally proposed by Frank.[11] The model has an inflow of reactants and an outflow of products and shows that a symmetric steady state becomes unstable and evolves to one of the two possible asymmetric steady states. A real chemical system in which chiral symmetry breaking occurs in accordance with the specific reaction steps in the Kondepudi−Nelson's model, however, has yet to be realized. In this article, a kinetic model to explain the chiral symmetry breaking transition in the growth front of a conglomerate crystal phase of 1,1′-binaphthyl is formulated. This model contains a chirally autocatalytic step, as in the Kondepudi−Nelson model but does not contain a cross-inhibition between the enantiomers. Also, as will be explained in detail below, the transition to asymmetric states does not occur through a bifurcation or branching of asymmetric state from the symmetric state; it occurs as a "hard transition" from one state to another.

The experimental background[15] for the model is the following. The chiral compound 1,1′-binaphthyl crystallizes in two forms: the racemic form, in which there are equal amounts of *R* and *S* enantiomers in each pure single crystal, and the chiral form, in which each pure single crystal has exclusively *R* or *S* enantiomers. Melting points of the racemic and chiral forms of 1,1′-binaphthyl are 145 and 158 °C, respectively.[12,13] Thus, the racemic form does not crystallize when the crystallization temperature is above 145 °C. In addition, the rate of racemization of 1,1′-binaphthyl is very high in the liquid phase, with a racemization half-life of about 0.5 s near its melting point of 158 °C.[14] Hence, when crystallization is performed at temperatures above 145 °C, a racemic liquid converts to a chiral crystal. But this does not imply that if we remove a crystal from a supercooled melt (above 145 °C), it will be 100% *R* or *S*. During the growth of a macroscopic crystal, *R* nuclei might form on a *S* surface and vice versa. Hence, each macroscopic crystal might have an enantiomeric excess (EE) less than 100%. If the rate of formation of *R* nuclei on an *S*-crystal surface is low, then we might expect a high EE. In our previous report of experimental results, crystals of 1,1′-binaphthyl, nucleated and grown above 145 °C (a temperature at which no racemic crystals can form) were carefully removed from the supercooled melt, and their EE was measured. The distribution of EE among these

* Corresponding author. Tel: +81-45-566-1553. Fax: +81-45-566-1560. E-mail: asakura@applc.keio.ac.jp.
† Keio University.
‡ Wake Forest University.

10.1021/jp0470041 CCC: $30.25
Published on Web 01/06/2005

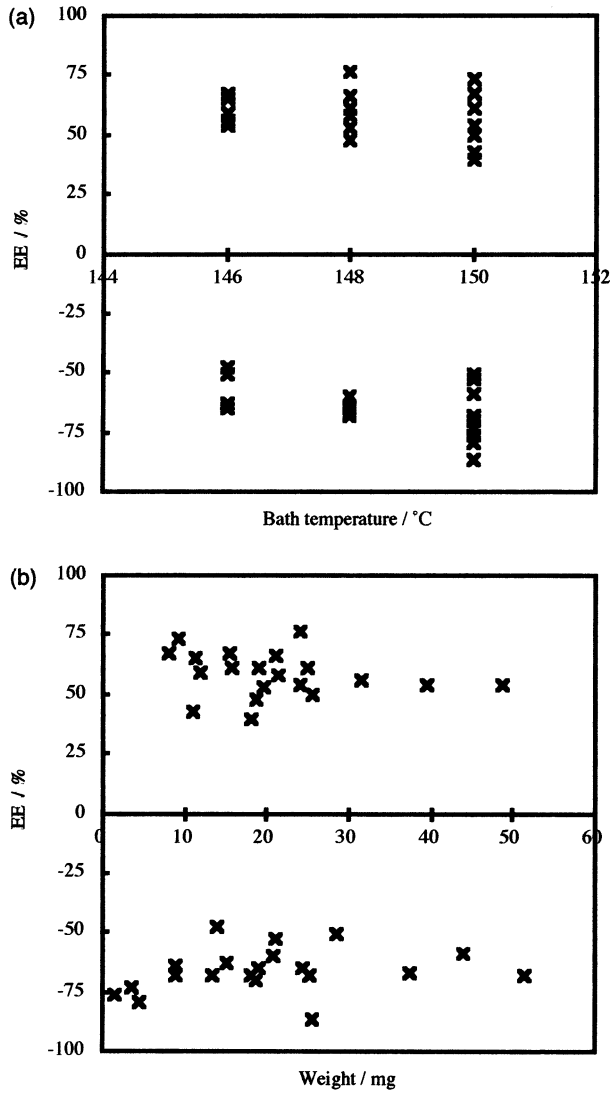

Figure 1. (a) Bimodal distribution observed in EE of growing crystal phases of 1,1′-binaphthyl generated in the supercooled melt. (b) Size independence of EE of growing crystal phases of 1,1′-binaphthyl generated in the supercooled melt. Unlike Figures 4 and 6 of our previous report,[15] only the data for the crystal phases that were characterized to consist of chiral crystallites exclusively by X-ray diffraction analysis are shown in this figure.

ensembles of crystallites was found to be bimodal, as shown in Figure 1a. Even in the case of bimodal distribution, the EE is not 100%, indicating that the solid phase is not 100% *R* or *S*. Because the crystallization temperature is well above 145 °C, the low EE could not be due to the racemic form of the crystal. This was further confirmed by X-ray diffraction, which can clearly distinguish between racemic and chiral forms of the solid; the X-ray diffraction results ruled out the possibility of a racemic form of the crystals in the solid phase for crystallization above 145 °C.[15] Hence, lower than 100% EE must be due to the formation of both *R* and *S* nuclei on the growing crystal surface. The crystals have very low EE, essentially zero, if the crystallization is done at a lower temperature. X-ray diffraction has confirmed that these crystals are racemic, not aggregates of chiral *R* and *S* crystallites.

The growth front of a crystallizing phase may be viewed as an open system.[15] The liquid phase at a higher chemical potential is flowing into the growth front and the solid at a lower chemical potential is flowing out of the front. In addition, surface nucleation has the chirally autocatalytic properties needed for chiral symmetry breaking. A growth front that maintains constant EE is a clear signature of open systems in the steady state. When chiral symmetry breaking occurs in an open system, the asymmetric state is maintained by the flows; the symmetric state of equal amounts of *R* and *S* is unstable whereas the asymmetric state of unequal amounts of *R* and *S* is stable. A bimodal distribution in the EE of an ensemble of crystallites is a characteristic of chiral-symmetry-breaking transition in which the probability of *R* or *S* dominance is 50%, an aspect that is evident in the experimental results shown in Figure 1a. Another characteristic is the stability of the state; the EE should not depend on the mass of the crystal (i.e., the EE should be maintained during crystal growth). Figure 1b shows a plot of mass of crystal versus EE. It indicates that the EE is essentially independent of the crystal mass.[15]

The model proposed in this article basically identifies the conditions under which the chirally autocatalytic surface nucleation can lead to the propagation of a chirally asymmetric solidification front in a supercooled melt. Unlike the previous models,[9,10] there is no cross-inhibition between *R*- and *S*-enantiomers in the model, because the solid phase of each enantiomer may not inhibit the nucleation of the other enantiomer. If the chiral autocatalysis is first order, a cross-inhibition reaction between the two enantiomers is also required for the chiral-symmetry-breaking transition. The system, however, might be able to spontaneously generate and maintain an asymmetric state depending on other factors without a cross-inhibition reaction if the chiral autocatalysis is of higher order.[2]

Kinetic Model

There are many theories for describing the mechanism of crystal growth. The growth of the ensemble of chiral crystallites of 1,1′-binaphthyl in the supercooled melt can be regarded in terms of the surface nucleation. A kinetic model was thus formulated according to the surface nucleation growth model.[16] In the model we propose, the growth of a crystal is viewed in terms of growth units, as it is usually done in models of crystal growth. A generation of the growth unit from the supercooled melt is a formation of partially ordered chiral aggregate on the crystal surface, and then the unit is incorporated into the crystal phase. Each growth unit can be *R* or *S*, a property that does not change once the unit is attached to the crystals. The growth units are classified into four types, depending on their location and character.

1. A growth unit already incorporated in the crystal bulk is surrounded on all sides by other growth units. The numbers of such growth units in the *S* and *R* configurations are denoted by C_S and C_R.

2. A growth unit at the crystal−melt interface on which another growth unit can attach belongs to the growth layer. The corresponding numbers of *S* and *R* units are denoted by I_S and I_R.

3. A growth unit in the growth layer is a partially ordered molecular aggregate. The numbers of *S* and *R* units in this layer are denoted by G_S and G_R.

Finally, the liquid phase is denoted by L; the "growth units" in this phase have no definite chirality because there is rapid interconversion between *R* and *S*.

A two-dimensional picture of the above layer by layer growth model is illustrated in Figure 2. The kinetics of crystal growth in above model is formulated as follows:

(a) L is transferred to G_S or G_R only on I, because homogeneous nucleation is usually negligibly slow when compared with surface nucleation. This process is represented

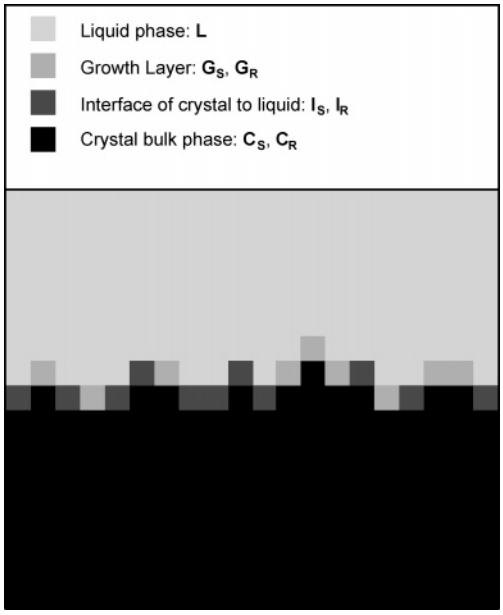

Figure 2. Schematic illustration of the layered growth model.

SCHEME 1: Whole Processes for the Kinetic Model of the Growth Front of Conglomerate Crystal Phase

$$\mathbf{L} + \mathbf{I_S} \xrightarrow{k_{01}} \mathbf{G_S} + \mathbf{C_S}$$
$$\mathbf{L} + \mathbf{I_R} \xrightarrow{k_{01}} \mathbf{G_R} + \mathbf{C_R}$$

$$\mathbf{L} + \mathbf{I_S} \xrightarrow{k_{02}} \mathbf{G_R} + \mathbf{C_S}$$
$$\mathbf{L} + \mathbf{I_R} \xrightarrow{k_{02}} \mathbf{G_S} + \mathbf{C_R}$$

$$\mathbf{L} + \mathbf{I_S} + \mathbf{G_S} \xrightarrow{k_{11}} 2\,\mathbf{G_S} + \mathbf{C_S}$$
$$\mathbf{L} + \mathbf{I_R} + \mathbf{G_R} \xrightarrow{k_{11}} 2\,\mathbf{G_R} + \mathbf{C_R}$$

$$\mathbf{L} + \mathbf{I_S} + \mathbf{G_R} \xrightarrow{k_{12}} \mathbf{G_S} + \mathbf{G_R} + \mathbf{C_S}$$
$$\mathbf{L} + \mathbf{I_S} + \mathbf{G_R} \xrightarrow{k_{12}} 2\,\mathbf{G_R} + \mathbf{C_S}$$
$$\mathbf{L} + \mathbf{I_R} + \mathbf{G_S} \xrightarrow{k_{12}} 2\,\mathbf{G_S} + \mathbf{C_R}$$
$$\mathbf{L} + \mathbf{I_R} + \mathbf{G_S} \xrightarrow{k_{12}} \mathbf{G_S} + \mathbf{G_R} + \mathbf{C_R}$$

$$\mathbf{L} + \mathbf{I_S} + \mathbf{G_S} \xrightarrow{k_{13}} \mathbf{G_S} + \mathbf{G_R} + \mathbf{C_S}$$
$$\mathbf{L} + \mathbf{I_R} + \mathbf{G_R} \xrightarrow{k_{13}} \mathbf{G_S} + \mathbf{G_R} + \mathbf{C_R}$$

$$\mathbf{G_S} \xrightarrow{k_{20}} \mathbf{I_S}$$
$$\mathbf{G_R} \xrightarrow{k_{20}} \mathbf{I_R}$$

as, L + I → C + G. The rate of generation of G_S on I_S is faster than the rate of generation of G_R on I_S, because the former has less interfacial energy. It is similar for the generation of G_S or G_R on I_R. This is a first-order chiral autocatalysis. Also, in this "reaction", I_S and I_R convert to C_S and C_R respectively.

(b) In addition to this first-order chiral autocatalysis, there is a second-order chiral autocatalysis in this model when we consider the addition of a growth unit that attaches to I and G; i.e., the one face of the growth unit attaches to an I-growth unit and another to a G-growth unit. This process can be written as, L + I + G → C + 2G. In this step, the chiralities of both I and G determine the chirality of the newly added growth unit, and hence its autocatalysis is effectively second-order.

(c) When molecules in the G-unit that are partially ordered are completely ordered, the G-unit is converted to an I-unit on which a new G-unit can be nucleated. This process is denoted by G → I.

The detailed kinetics of various combinations of *R* and *S* units in the above sets of reactions is shown in Scheme 1. This scheme contains all the possible reaction steps that result in conversions of L to G, G to I, and I to C.

Based on Scheme 1, kinetic equations for the chiral composition of system consisting of I- and G-units, can be formulated. In these equations, "L", which is the liquid phase, does not appear. The rate at which L is converted to G depends on the supercooling. It is thus included in the kinetic rate constants and does not appear explicitly. The conversion of L to G is an inflow into the system consisting of I- and G-units. The conversion of I-units to C-units is an outflow from the system. Thus, in this system, there is an inflow and an outflow of growth units. The system variables are I_S, I_R, G_S, and G_R. For this four-variables kinetic model, the following set of four kinetic equations, (1)−(4), can be written under the assumption that k_{02} and k_{13} are negligibly small.

$$\frac{dG_S}{dt} = k_{01}I_S + k_{11}I_SG_S + k_{12}(I_SG_R + I_RG_S) - k_{20}G_S \quad (1)$$

$$\frac{dG_R}{dt} = k_{01}I_R + k_{11}I_RG_R + k_{12}(I_SG_R + I_RG_S) - k_{20}G_R \quad (2)$$

$$\frac{dI_S}{dt} = -k_{01}I_S - k_{11}I_SG_S - 2k_{12}I_SG_R + k_{20}G_S \quad (3)$$

$$\frac{dI_R}{dt} = -k_{01}I_R - k_{11}I_RG_R - 2k_{12}I_RG_S + k_{20}G_R \quad (4)$$

In this system, it is easy to see that the quantity $G_S + G_R + I_S + I_R$ is a constant. Steady-state solutions can be obtained by setting all the equations to zero. Also, by adding (1) and (3) we see that

$$\frac{d(G_S + I_S)}{dt} = k_{12}(I_RG_S - I_SG_R) = 0 \quad (5)$$

at the steady state. Hence, for all steady states

$$I_RG_S = I_SG_R \quad (6)$$

For a symmetric steady state, $I_S = I_R$ and $G_S = G_R$. Substituting (6) in (1), we see that

$$k_{01}I_S + k_{11}I_SG_S + 2k_{12}I_SG_S - k_{20}G_S = 0 \quad (7)$$

from which one can obtain the following relation between I_S and G_S:

$$G_S = \frac{k_{01}I_S}{-k_{11}I_S - 2k_{12}I_S + k_{20}} \quad (8)$$

For the above set of kinetic equations, explicit steady-state solutions can be obtained as follows. Because $G_S + G_R + I_S + I_R \equiv T$ is a constant, we can normalize the concentrations such that $G_S + G_R + I_S + I_R = 1$. In these normalized variables, for the symmetric steady state (in which the number of *S*-units equals number of *R*-units), $G_S + I_S = G_R + I_R = 0.5$. Now the

set of equations (1)−(4) can be explicitly solved to obtain the following symmetric steady state:

$$G_S = G_R = \left[-2k_{01} + k_{11} + 2k_{12} - 2k_{20} + \sqrt{(2k_{01} - k_{11} - 2k_{12} + 2k_{20})^2 + 4(2k_{11} + 4k_{12})k_{01}}\right] \Big/ \left[2\left(2k_{11} + 4k_{12}\right)\right]$$

$$I_S = I_R = \left[2k_{01} + k_{11} + 2k_{12} + 2k_{20} - \sqrt{(2k_{01} - k_{11} - 2k_{12} + 2k_{20})^2 + 4(2k_{11} + 4k_{12})k_{01}}\right] \Big/ \left[2\left(2k_{11} + 4k_{12}\right)\right] \quad (9)$$

Similarly, we can also obtain the following asymmetric steady-state solutions:

$$G_S = \frac{k_{01} I_S}{-k_{11} I_S + k_{20}}$$

$$G_R = I_R = 0 \quad (10)$$

$$G_R = \frac{k_{01} I_R}{-k_{11} I_R + k_{20}}$$

$$G_S = I_S = 0 \quad (11)$$

If we use the same normalization, $G_S + G_R + I_S + I_R = 1$ as we did for the symmetric steady states, (10) and (11) give

$$G_S = \frac{-k_{01} + k_{11} - k_{20} + \sqrt{(k_{01} - k_{11} + k_{20})^2 + 4k_{01}k_{11}}}{2k_{11}}$$

$$I_S = \frac{k_{01} + k_{11} + k_{20} - \sqrt{(k_{01} - k_{11} + k_{20})^2 + 4k_{01}k_{11}}}{2k_{11}}$$

$$G_R = I_R = 0 \quad (12)$$

$$G_S = I_S = 0$$

$$G_R = \frac{-k_{01} + k_{11} - k_{20} + \sqrt{(k_{01} - k_{11} + k_{20})^2 + 4k_{01}k_{11}}}{2k_{11}}$$

$$I_R = \frac{k_{01} + k_{11} + k_{20} - \sqrt{(k_{01} - k_{11} + k_{20})^2 + 4k_{01}k_{11}}}{2k_{11}} \quad (13)$$

The two sets of asymmetric solutions (12) and (13) are, as we expect, "mirror images" of each other. A point to note about the above symmetric and asymmetric steady states is that they do not intersect. Hence the transition from one to another is not a "branching" or "bifurcation" of steady states.

In conclusion, we see that the above model leads to both symmetric and asymmetric steady-state solutions. Which one the system will settle into under given conditions depends on the stability of these steady states. To determine the stability, we need to do a linear stability analysis.

Linear Stability Analysis

The symmetric or asymmetric steady state can be realized during the growth process, only if it is stable. The usual linear stability analysis[1,3] can be performed for the above two steady states. The stability of a steady state depends on the eigenvalues of the Jacobian matrix, (14), evaluated at the steady state. The steady state under consideration is stable only if all eigenvalues have negative real parts. Four eigenvalues of the Jacobian matrix for asymmetric solutions were calculated by substituting (12) into (14) using Mathematica. We shall denote the four eigenvalues by λ_k, $k = 1, 4$. We can obtain analytical expressions for two eigenvalues: $\lambda_1 = 0$ and $\lambda_2 = -\sqrt{(k_{01}-k_{11}+k_{20})^2+4k_{01}k_{11}}$. Thus, neither λ_1 nor λ_2 have a positive real part. The other two eigenvalues, λ_3 and λ_4, as functions of k_{11} were calculated using Mathematica for $k_{20} = 0.002$, 0.005, and 0.01. By considering the interfacial energies involved in the attachment of a growth unit, we can establish the following relation between the rate constants: $k_{01} < k_{12} < k_{11}$. To simplify the linear stability analysis, we set $k_{01} = 0.001$ and $k_{12} = 0.002$.

Eigenvalues, λ_3 and λ_4, as functions of k_{11} thus calculated are shown in Figure 3. λ_3 was found to be always a negative real number, whereas λ_4 changes sign depending on the value of k_{11}. For a given set of kinetic constants, only one of the steady states, symmetric or asymmetric, is found to be stable. If the kinetic constants are varied, there is a "critical point" at which the stability shifts from symmetric solution to the asymmetric and vice versa depending on how the kinetic constant is changed, increased or decreased. For the asymmetric steady state, the critical point was found at $k_{11} = 0.004$; when $k_{11} > 0.004$ the asymmetric solution is stable, but it becomes unstable when $k_{11} < 0.004$. The stability of the solution is thus independent of the value of k_{20} (which is the rate constant for the process incorporating the growth layer units into the crystal phase).

For symmetric solutions, the real parts of the eigenvalues of the Jacobian matrix calculated by substituting (9) into (14) are shown in Figure 4. The three eigenvalues, λ_1, λ_2, and λ_3, do

$$\mathbf{J} = \begin{bmatrix} \frac{\partial(\mathrm{d}G_S/\mathrm{d}t)}{\partial G_S} & \frac{\partial(\mathrm{d}G_S/\mathrm{d}t)}{\partial G_R} & \frac{\partial(\mathrm{d}G_S/\mathrm{d}t)}{\partial I_S} & \frac{\partial(\mathrm{d}G_S/\mathrm{d}t)}{\partial I_R} \\ \frac{\partial(\mathrm{d}G_R/\mathrm{d}t)}{\partial G_S} & \frac{\partial(\mathrm{d}G_R/\mathrm{d}t)}{\partial G_R} & \frac{\partial(\mathrm{d}G_R/\mathrm{d}t)}{\partial I_S} & \frac{\partial(\mathrm{d}G_R/\mathrm{d}t)}{\partial I_R} \\ \frac{\partial(\mathrm{d}I_S/\mathrm{d}t)}{\partial G_S} & \frac{\partial(\mathrm{d}I_S/\mathrm{d}t)}{\partial G_R} & \frac{\partial(\mathrm{d}I_S/\mathrm{d}t)}{\partial I_S} & \frac{\partial(\mathrm{d}I_S/\mathrm{d}t)}{\partial I_R} \\ \frac{\partial(\mathrm{d}I_R/\mathrm{d}t)}{\partial G_S} & \frac{\partial(\mathrm{d}I_R/\mathrm{d}t)}{\partial G_R} & \frac{\partial(\mathrm{d}I_R/\mathrm{d}t)}{\partial I_S} & \frac{\partial(\mathrm{d}I_R/\mathrm{d}t)}{\partial I_R} \end{bmatrix}$$

$$= \begin{bmatrix} k_{11}I_S + k_{12}I_R - k_{20} & k_{12}I_S & k_{01} + k_{11}G_S + k_{12}G_R & k_{12}G_S \\ k_{12}I_R & k_{11}I_R + k_{12}I_S - k_{20} & k_{12}G_R & k_{01} + k_{11}G_R + k_{12}G_S \\ -k_{11}I_S + k_{20} & -2k_{12}I_S & -k_{01} - k_{11}G_S - 2k_{12}G_R & 0 \\ -2k_{12}I_R & -k_{11}I_R + k_{20} & 0 & -k_{01} - k_{11}G_R - 2k_{12}G_S \end{bmatrix} \quad (14)$$

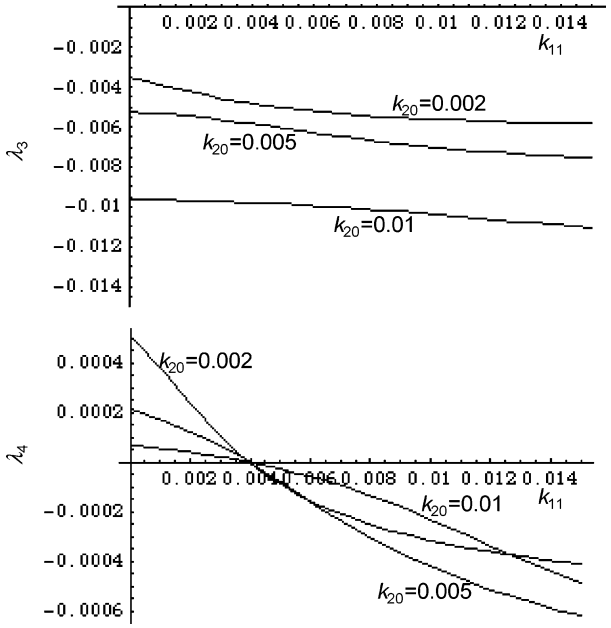

Figure 3. Real part of two of the four eigenvalues of the Jacobian matrix of the kinetic model for the asymmetric steady-state solution as functions of k_{11}.

not have a positive real part, whereas the fourth, λ_4, changes sign at $k_{11} = 0.004$. The critical point of λ_4 is thus the same as the one for the asymmetric solution and it is also independent of the value of k_{20}. Furthermore, in contrast to the asymmetric solutions, the symmetric solutions are stable when $k_{11} < 0.004$, but become unstable when $k_{11} > 0.004$. As can be seen from Scheme 1, the value of k_{11} can be regarded as the strength of chiral autocatalysis. As one might expect, the above results indicate that the symmetric state is stable when the strength of chiral autocatalysis is low but it becomes unstable when the strength becomes high; this instability drives the system to the one of the two asymmetric states.

Numerical Simulation

Validity of the linear stability analysis was checked by numerical simulations of the kinetic equations (1)−(4). We used the parameter values $k_{01} = 0.001$, $k_{12} = 0.002$, and $k_{20} = 0.002$, 0.005, or 0.01. Simulations were carried out below and above the critical point by setting the strength of chiral autocatalysis as $k_{11} = 0.003$ or 0.005. When $k_{11} = 0.003$, which is below the critical point, initial conditions for the simulation were $G_{S0} = 0.49$, $G_{R0} = 0.01$, $I_{S0} = 0.49$, and $I_{R0} = 0.01$, i.e., conditions slightly perturbed from the asymmetric steady state. On the other hand, when $k_{11} = 0.005$, which is above the critical point, initial conditions were $G_{S0} = 0.26$, $G_{R0} = 0.24$, $I_{S0} = 0.25$, and $I_{R0} = 0.25$, conditions slightly perturbed from the symmetric steady state.

Figure 5 shows the result of the simulation in which $k_{11} = 0.003$. In all cases, each variable asymptotically approaches the symmetric solution where $G_S = G_R$ and $I_S = I_R$. As we noted above, linear stability analysis indicated that the symmetric solution is stable but the asymmetric solution is unstable for these values of the rate constants. The result of the numerical simulation is thus consistent with the result of linear stability analysis. When $k_{11} = 0.005$, the variables asymptotically approach the asymmetric solution where $G_S + I_S = 1$ and $G_R = I_R = 0$, as shown in Figure 6. This result is also consistent with the result of linear stability analysis.

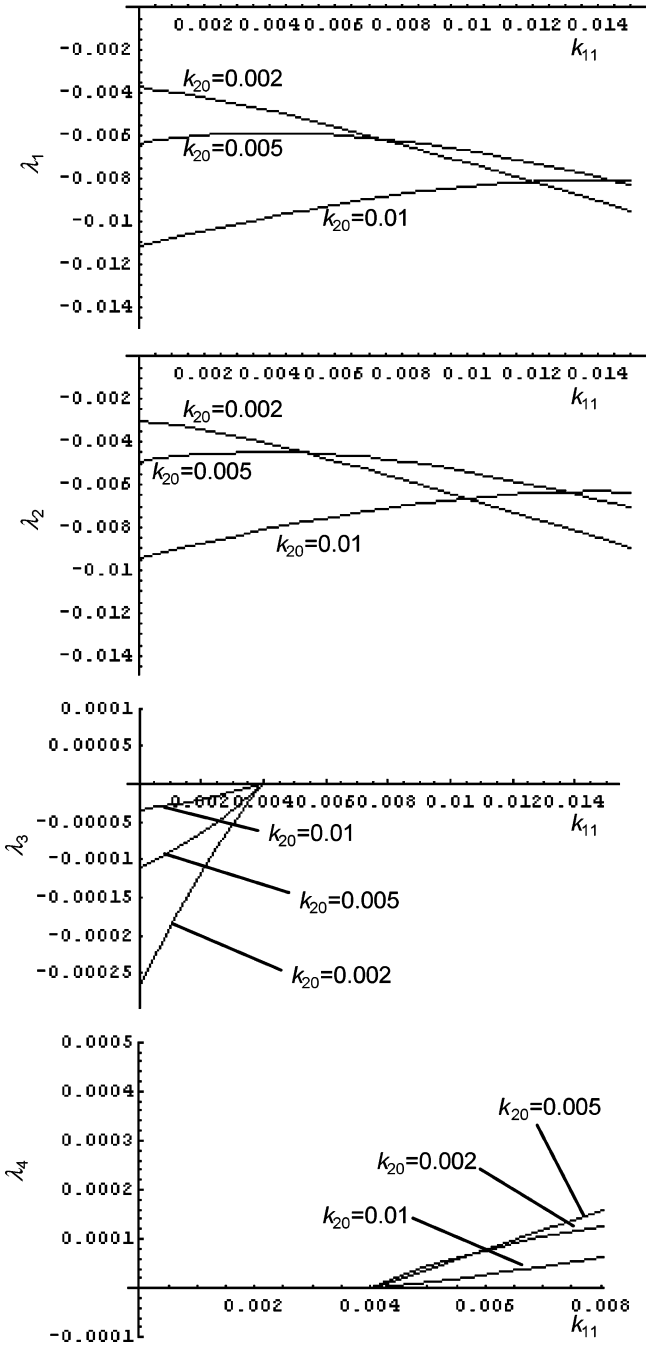

Figure 4. Real part of the four eigenvalues of the Jacobian matrix of the kinetic model for the symmetric steady-state solution as functions of k_{11}.

The ratio of $(G_S + G_R)$ to $(I_S + I_R)$ at the stable steady state decreases with increasing value of the rate constant k_{20}. In addition, the rate of transition to the stable steady state was influenced by k_{20}; as k_{20} increases, longer time was required for the transition.

Conclusion

Kondepudi and Nelson formulated a general theory of chiral symmetry breaking as an example of dissipative structure in open system in the 1980s.[9,10] To illustrate this process, they used a modification of a model proposed by Frank.[11] In this article, we have noted how an open system can effectively be realized in the case of crystal growth. This analysis was undertaken because we recently found that the crystal growth

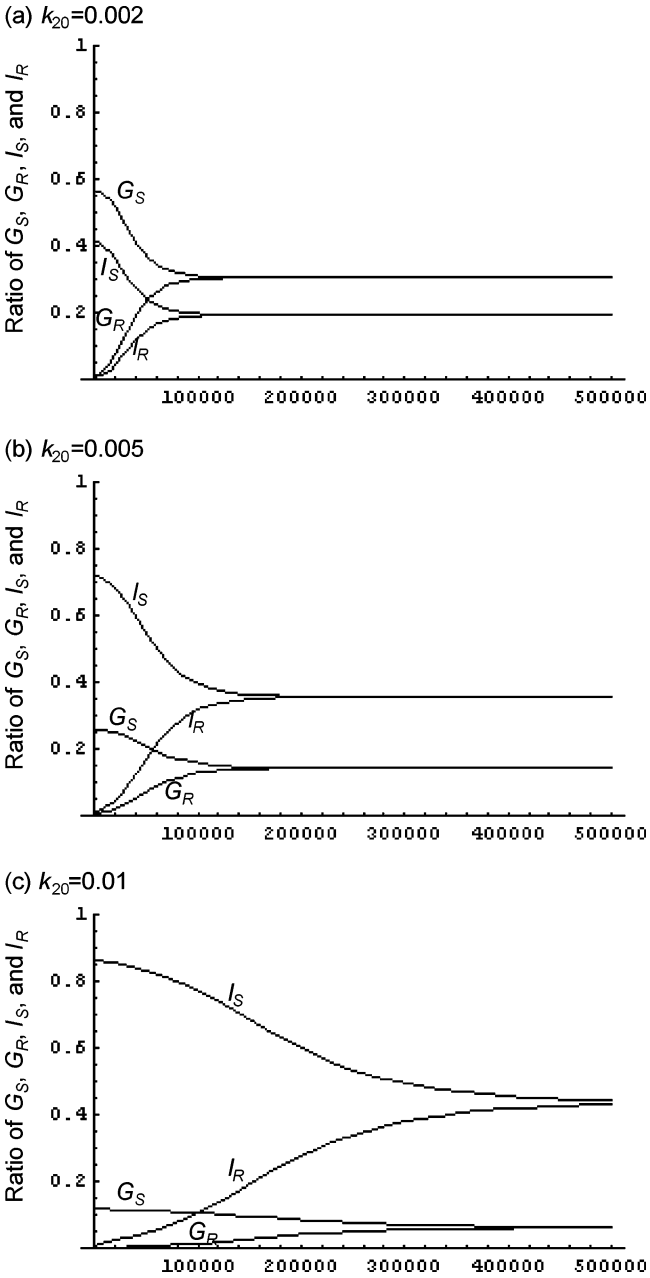

Figure 5. Numerical simulations starting from conditions slightly perturbed from the asymmetric steady state, $G_{S0} = 0.49$, $G_{R0} = 0.01$, $I_{S0} = 0.49$, and $I_{R0} = 0.01$. In this case, $k_{11} = 0.003$ at which symmetric steady-state solutions is stable but asymmetric steady-state solutions are unstable.

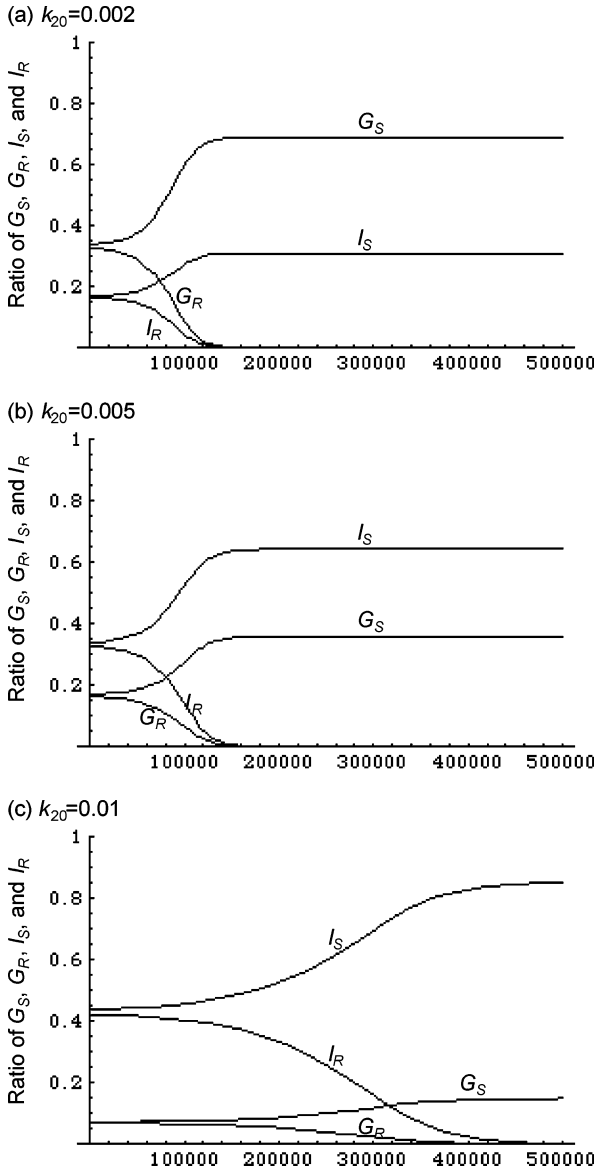

Figure 6. Numerical simulations starting from conditions slightly perturbed from the symmetric steady state, $G_{S0} = 0.26$, $G_{R0} = 0.24$, $I_{S0} = 0.25$, and $I_{R0} = 0.25$. In this case, $k_{11} = 0.005$, at which asymmetric steady-state solutions are stable but symmetric steady-state solution is unstable.

front of 1,1′-binaphthyl shows many of the characteristics of an open system in which chiral symmetry breaking has occurred.[15] A kinetic model to explain the mechanism of chiral symmetry breaking transition in the growth front of the 1,1′-binaphthyl solid phase in its supercooled melt is formulated. In this model, a pair of asymmetric and symmetric steady-state solutions that do not intersect were found. These two steady states exchange stability (i.e., when the symmetric state becomes unstable, the asymmetric state becomes stable and vice versa), but the exchange of stability does not occur at a point at which the two solutions intersect. Linear stability analysis enabled us to identify a critical point as a function of the strength of chiral autocatalytic step in the model. At this critical point, numerical simulation confirmed that a transition from one steady state to another occurs. Thus, we have shown that the growth front of a 1,1′-binaphthyl is effectively an open system in which chiral symmetry breaking can be realized.

Acknowledgment. We thank grant from Japan Space Forum (15JSF-14026), Grant-in-Aid for Scientific Research (C) from Japan Society for Promotion of Science (4830), and Grant-in-Aid for the 21st Century COE program "Keio Life Conjugate Chemistry" from the Ministry of Education, Culture, Sports, Science, and Technology, Japan for supporting this work.

References and Notes

(1) Kondepudi, D. K.; Prigogine, I. *Modern Thermodynamics −From Heat Engines to Dissipative Structure*; John Wiley & Sons: New York, 1998.

(2) Kondepudi, D. K.; Asakura, K. *Acc. Chem. Res.* **2001**, *34*, 946.

(3) Epstein, I. R.; Pojman, J. A. *An Introduction to Nonlinear Chemical Dynamics −Oscillations, Waves, Patterns, and Chaos*; Oxford University Press: New York, 1998.

(4) Prigogine, I.; Lefever, R. *J. Chem. Phys.* **1968**, *48*, 1695.

(5) Noyes, R. M.; Field, R. J.; Koros, E. *J. Am. Chem. Soc.* **1972**, *94*, 1394.

(6) Belousov, B. P. *A Periodic Reaction and Its Mechanism* in *Sbornik Referatov po Radiatsionni Meditsine*; Med Publ.: Mowcow, 1958; p 145.

(7) Turing, A. M. *Philos. Trans. R. Soc. London* **1952**, *237B*, 37.

(8) Castets, V.; Dulos, E.; Boissonade, J.; De Kepper, P. *Phys. Rev. Lett.* **1990**, *64*, 2953.

(9) Kondepudi, D. K.; Nelson, G. W. *Physica A* **1984**, *125*, 465.

(10) Kondepudi D. K.; Nelson G. W. *Nature* **1985**, *314*, 438.

(11) Frank, F. C. *Biochim. Biophys. Acta* **1953**, *11*, 459.

(12) Badar, Y.; Ling, C. C. K.; Cooke, A. S.; Harris, M. *J. Chem. Soc.* **1965**, 1543.

(13) Kress, R. B.; Duesler, E. N.; Etter, M. C.; Paul, I. C.; Curtin, D. Y. *J. Am. Chem. Soc.* **1980**, *102*, 7709.

(14) Cooke, A. S.; Harris, M. M. *J. Chem. Soc.* **1963**, 2365.

(15) Asakura, K.; Nagasaka, Y.; Hidaka, M.; Hayashi, M.; Osanai, S.; Kondepudi, D. K. *Chirality* **2004**, *16*, 131.

(16) Randolph, A. D.; Larson, M. D. *Theory of Particulate Processes*, 2nd ed.; Academic Press: San Diego, 1991.